Electronic Supplementary Material (ESI) for Soft Matter.

Supporting information for *Rheology of Soft Colloids Near Rigidity Onset: Critical Scaling, Thermal, and Non-thermal Responses*

Anindita Basu,[1] Ye Xu,[1,2] Tim Still,[1,2] P. E. Arratia,[3] Zexin Zhang,[4] K. N. Nordstrom,[1] Jennifer M. Rieser,[1] J. P. Gollub,[1,5] D. J. Durian,[1] and A. G. Yodh[1]

[1] *Department of Physics and Astronomy,*
University of Pennsylvania, PA 19104, USA
[2] *Complex Assemblies of Soft Matter,*
CNRS-Rhodia-UPenn UMI 3254, Bristol, Pennsylvania 19007, USA
[3] *Department of Mechanical Engineering and Applied Mechanics,*
University of Pennsylvania, PA 19104, USA
[4] *Center for Soft Condensed Matter Physics and Interdisciplinary Research,*
Soochow University, Suzhou, China
[5] *Department of Physics, Haverford College, PA 19041, USA*

(Dated: January 16, 2014)

PACS numbers:

I. YOUNG'S MODULI OF THE PNIPAM PARTICLES

Centrifugal compression experiments are carried out following the procedure described in Nordstrom *et al.* [1] in order to estimate the Young's moduli of the ∼700 nm monodisperse PNIPAM microgel particles used in the experiments. Specifically, PNIPAM suspensions are loaded and sealed in glass tubes with diameter of 2 mm. The tubes are then loaded into a thermostated centifuge (Marathon 21000R), and the samples are allowed to settle at a fixed angular rotation speed. Measurements are made at five rotation speeds (RCF$= \omega^2 R/g =$ 100, 200, 300, 400, and 500) at two temperatures (T=291 K and 295 K). Here ω is the angular rotation speed, R is the distance between the rotation center and the sample, and g is the gravitational acceleration. The heights of compressed PNIPAM particle packings are recorded and plotted in Fig. S1. By fitting the data to Eq. (21) in Nordstrom *et al.* [1], the Young's moduli of PNIPAM particles are estimated to be 8 kPa at 291 K and 25 kPa at 295 K. We note that these particles are ∼ 50 % softer than those used in Ref. [2] (Young's moduli of the slightly larger PNIPAM particles, ∼1 μm, used in the microfluidic experiments were 15 kPa at 291 K and 45 kPa at 295 K).

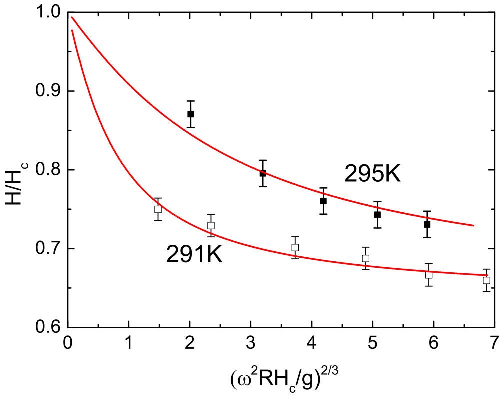

FIG. S1: (Color online) Compressed particle packing height versus acceleration. The height, H, is scaled by H_c, the initial height without compression pressure. Filled-in and open symbols are measurements at 295K and 191K, respectively. The two red lines are the fit to Eq. (21) in Ref. [2]. Centrifugal measurements were carried out on mono-disperse PNIPAM suspensions (∼700 nm).

II. WALL-SLIP EFFECT

We have also checked for wall-slip effects by introducing surface roughness into our steady-state viscometry measurements. The rheometer tools are roughened by sintering polystyrene (PS) micro-spheres, ∼800 nm diameter (Seradyn Microparticle Technology, US), on the surfaces of the rheometer cone and plate. Fig. S2(a) shows a scanning electron micrograph with back-scattered electron detection capability (Quanta 600 scanning electron microscope, FEI, USA) to image the PS micro-spheres sintered on their surface at 1000× magnification (Inset - 2000× magnification).

Using the roughened tools, we compare σ of a batch of slightly larger PNIPAM (≈800 nm diameter) microgel suspension for a range of $\dot{\gamma} = 0.005 \rightarrow 5$ 1/s, as seen in Figs. S2(b). The open symbols in the figure indicate data taken *without* roughened rheometer tools; filled-in symbols of the same color plot the corresponding data-set measured *with* roughened rheometer tools. Measurements are made at different temperatures corresponding to different volume fractions above and below the liquid-solid transition. The dataset is restricted to $Re \lesssim 0.5$, as is the case in all of our experiments. We note that there are small differences in the measured stress obtained with versus without surface roughening. This observation suggests that wall slip effects in our system are not likely to be large. In fact, we can derive a reasonable scaling collapse of σ and $\dot{\gamma}$ from these data using the χ^2-minimization fitting scheme. Both datasets exhibit critical scaling behavior when scaled using the critcal scaling exponents, $\Delta \approx$ 2.5 and $\Gamma \approx$ 5 reported in the paper, and $T_c \approx$ 297 K (figures not shown).

To further show that the wall-slip effect is not significant in our system, we explored the velocity profile data from microfluidics experiments in Nordstrom *et al.* [2] and extracted the slip lengths for various packing fractions and shear rates, as shown in Fig. S3. First, finite values of slip lengths were observed for $\phi > \phi_c$, and the slip lengths generally increased with ϕ. This finding is consistent with control experiments in Fig. S2, wherein the difference in measured stresses for smooth and rough surfaces increased with ϕ. Second, the slip lengths are of the order of 5μm to 20μm. Since the slip length is a materials parameter that depends on the properties of colloidal particles and the surface roughness, it is reasonable to assume that the slip lengths would not change too much in our macrorheology setup with smooth surfaces. In this case, the scale of the slip lengths is very small compared to the average gap between the cone-shape head and the bottom plate of our rheometer, which is about 1.4 mm.

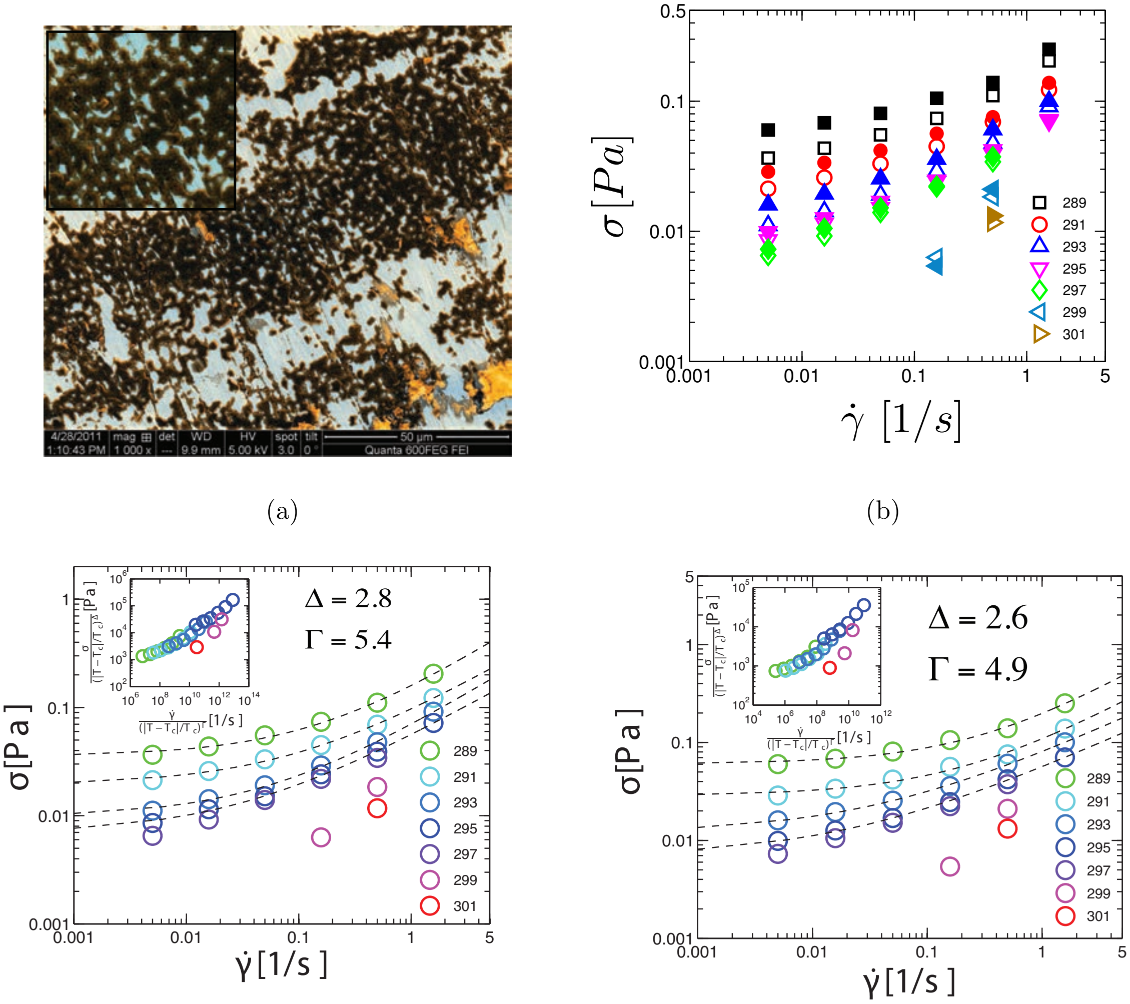

(a)

(b)

(c)

(d)

FIG. S2: (Color online) (a) Scanning electron micrograph at 1000× magnification of rheometer tools with 800 nm PS micro-spheres sintered on the surfaces (Inset - 2000× magnification). (b) σ vs. $\dot{\gamma}$ of a monodisperse PNIPAM suspension (diameter, ≈800 nm) using rheometer cone-and-plate without (open symbols), and with (filled-in symbols) surface roughening. (c) and (d) Same scaling analysis performed for data from smooth (c) and rough (d) surfaces. The scaling parameters, Δ and Γ show similar values.

This small slip-length to gap ratio, can explain (at least in part) the small difference between measured stresses with smooth and rough surface in Fig. S2 in the supporting information.

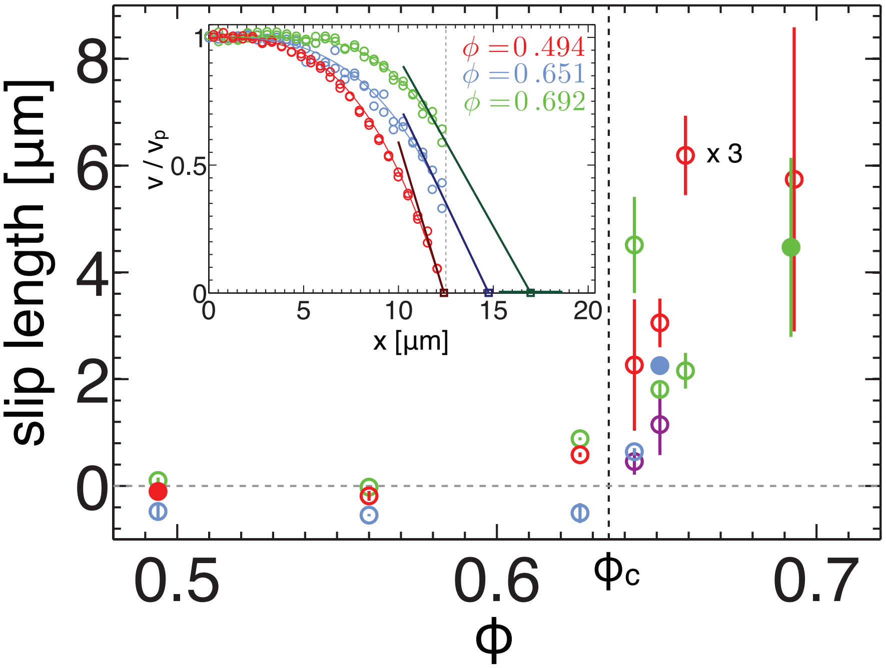

FIG. S3: (Color online) Slip lengths versus volume fraction, based on velocity profile data from Nordstrom *et al.* [2] Within each volume fraction, the colors red, green, blue, and purple indicate the relative driving pressure from smallest to largest. One possibly anomalous data point is outside the bounds of this plot: $\phi = 0.659$, slip length $= 19 \pm 3 \mu m$, which was scaled into the plot region by dividing by 3. The inset shows velocity profile data for three example volume fractions, as labeled, normalized by the peak speed at the center of the channel, $x = 0$. Fits to the functional form expected for $\sigma = \sigma_y + \sigma_0(\tau\dot{\gamma})^{1/2}$ are shown as thin solid curves. The lines tangent to the fits at the boundary, $x = 12.5\mu m$, are shown by heavy lines. The slip lengths are given by the distance outside the sample at which these lines hit the x-axis. The filled points in the main plot correspond to the extrapolations illustrated in the inset.

III. SHEAR HISTORY EFFECTS

Shear history can have significant impact on the rheological measurements of densely packed particle suspensions. It is therefore desirable to minimize shear history effects in rheology measurements. In order to confirm that the effect of shear history is minimal in our viscosity measurements, we conducted a control experiment on the monodisperse PNIPAM microgel suspension (∼700 nm) at $T = 293$ K. An extra pre-shear step was preformed where a high strain rate ($\dot{\gamma} = 20$ s $^{-1}$ for 10 seconds) was applied before the sample was tested at any given strain rate. A high strain rate applied before a viscosity measurement erases shear history to break up any flocs or transient particle clusters that may have formed from sample aging [3, 4]. We measured time-resolved shear stresses responding to four different shear rates with this extra pre-shear step, and compared with the results measured without any extra pre-shear. As shown in Fig. S4, despite some deviations at short time scale, the results suggest that the same steady states were reached independent of the pre-shear except small difference at the lowest shear rate.

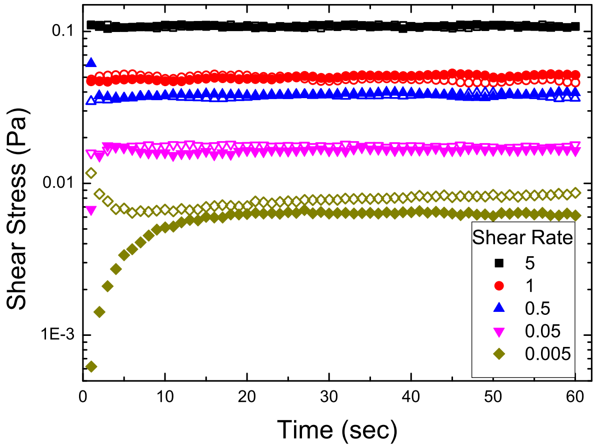

FIG. S4: (Color online) Shear stress versus time for monodisperse PNIPAM suspension (~700 nm) at different strain rates. Filled and open symbols are measurements with and without an applied pre-shear before testing at each shear rate, respectively. The sample responded differently to the same strain rate at short time scale and small strain region depending on whether a pre-shear was applied, but eventually reaches to the same plateau with similar steady-state shear stresses.

IV. CONTOUR PLOTS OF $log_{10}(\chi^2)$ VALUES OBTAINED FROM χ^2-MINIMIZATION FITTING SCHEME

Fig. S5 displays $log_{10}(\chi^2)$ values obtained from fitting $\sigma/(|T - T_c|/T_c)^\Delta$ vs. $\dot{\gamma}/(|T - T_c|/T_c)^\Delta$ (to a second-order polynomial on the jammed side, and a third-order polynomial on the unjammed side) in the form of contour plots. Δ, Γ, and T_c are fitting parameters, the values of which are varied between $1 \rightarrow 9$, $1 \rightarrow 9$, and $291 \rightarrow 299$ K, respectively, in steps of

0.1, 0.1 and 0.1 K. Data shown here is from the monodisperse PNIPAM sample ($\sim$700 nm).

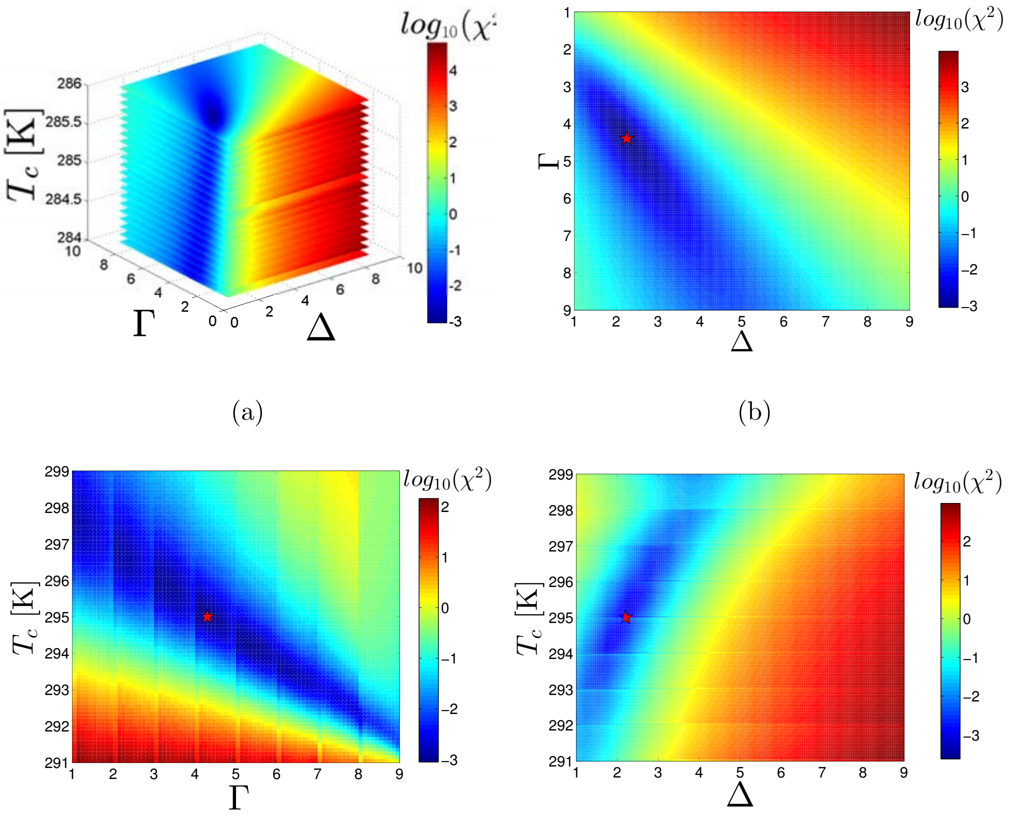

(a) (b)

(c) (d)

FIG. S5: (Color online) (a) 3D contour plot of $log_{10}(\chi^2)$ obtained from polynomial fits to the scaled rheology data for the monodisperse PNIPAM sample. Blue end of the color-bar indicates low χ^2. The minimum χ^2 is indicated by the red star. (b), (c) and (d) show a slice each taken from the 3D plot where (a) T_c is held constant at 295 K while the scaling exponents, Δ and Γ and made to vary, (b) Δ is held constant at 2.2 while T_c, Γ are varied, and (c) Γ is held constant at 4.3 while T_c, Δ are varied.

V. SCALING ANALYSIS USING HERSCHEL-BULKLEY FITTING

Following the fitting scheme [2], we fit the jammed data at each temperature using the Herschel-Bulkley (HB) model, $\sigma = \sigma_y + k\dot{\gamma}^n = \sigma_y \{1 + (\tau\dot{\gamma})^n\}$, where τ is a relaxation time-constant described by Nordstrom *et al.* [2]. As shown in Fig. 2 in the main paper, n is in agreement with the HB exponent reported by Nordstrom *et al.* [2]. Per scaling, we note that even though the viscometry data of the solid-like samples can be fit reasonably well to the HB model, the HB fitting schemes used to derive scaling exponents in Ref. [2] proved more difficult to apply to our macro-rheology data. For example, the macro-rheology experiments were unable to approach the liquid-solid transition as closely as the microfluidic experiments due to the limitations in temperature control when using the rheometer; thus we have fewer points very close to the transition point, and by comparison to our χ^2 minimization method, we only use half of the available data. Nevertheless, we perform the HB analysis for completeness sake in this section, as follows. We fix n at its mean value, and repeat the HB fits to obtain a new set of σ_y and k versus temperature. The timescale, τ, is derived from k such that $\tau = (\sigma_y/k)^n$. σ_y and τ are then fitted to power laws in $|T - T_c|$, where both exponent and critical temperature are adjusted. This gives two values of T_c, *viz.*, $(T_c)_{\sigma_y}$ and $(T_c)_k$, which are at most within a couple of degrees Kelvin of one another; our estimated critical temperature, T_c is obtained by averaging these two values, as $T_c = ((T_c)_{\sigma_y} + (T_c)_k)/2$. ϕ_c and ϕ are then calculated using Eqns. (1) and (2) in the main paper. σ_y and τ values are then plotted as functions of $|\phi - \phi_c|$ on log-log plots, the slopes of which give us the exponents Δ and Γ, respectively. (Δ obtained from power-law fit for σ_y vs. $(\phi_c)_{\sigma_y}$ and Γ similarly from power law fit for τ vs. $(\phi_c)_k$ are in agreement with Δ and Γ obtained from using average ϕ_c, within error bars.) Fig. S6 plots n, σ_y and τ for the monodisperse (a, b, c) and bidisperse (d, e, f) PNIPAM suspensions respectively.

Δ and Γ thus calculated are as follows: 1.3 ± 0.03 (fitting error) ± 0.2 (systematic error), and $1.6 \pm 0.13 \pm 0.3$ (monodisperse PNIPAM system); (b) $1.4 \pm 0.1 \pm 0.3$, and $1.0 \pm 0.1 \pm 0.3$ (bidisperse PNIPAM system). The systematic errors in Δ and Γ are calculated as following: The G_0 vs. $|\phi - \phi_c|$ fit is performed with the first 30% of data excluded, which yields an α, say α_1. The fit is performed again with the last 30% of the data-set excluded this time, yielding a different α, say α_2. The largest standard deviation between the α calculated for the entire data-set, and α_1 or α_2 gives the systematic error. Δ obtained from yield-stress scaling in monodisperse and *bidisperse* systems are roughly in agreement with the Δ values obtained from the χ^2-minimization method (within the error bars) and reported previously for monodisperse systems [2]. Values of Γ obtained from scaling the τ derived from the HB fits, however, appear to be systematically lower than the exponents reported in both [2, 5] and from the χ^2 minimization method. This discrepancy in Γ values may have its origin in

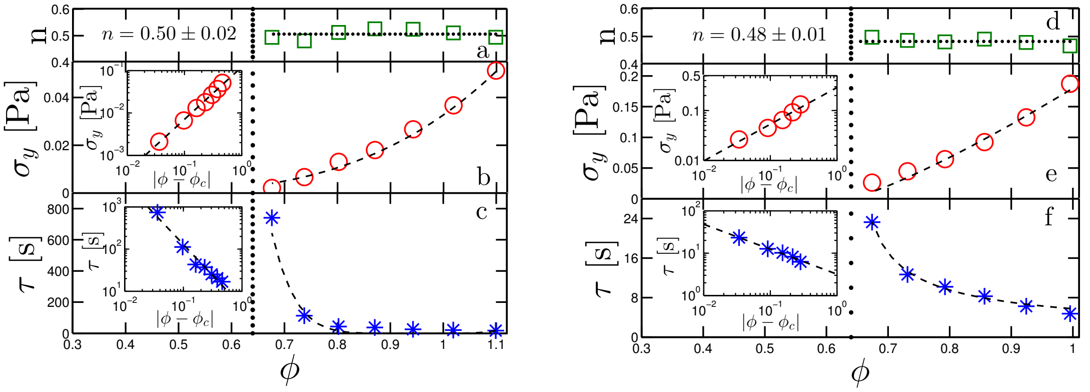

(a) Monodisperse

(b) Bidisperse

FIG. S6: (Color online) Scaling exponents Δ, Γ obtained from the HB fits to macro-rheology data for (a, b, c) monodisperse PNIPAM microgel suspensions (diameter, ~700 nm), and (d, e, f) bidisperse PNIPAM suspensions (diameters, ~500 nm, 700 nm). For the monodisperse and bidisperse systems, respectively, (a) and (d) plots the HB exponent, n as a function of ϕ, (b) and (e) plots σ_y Pa vs. ϕ (inset - σ_y Pa vs. $|\phi - \phi_c|$), and (c) and (f) plots τ s vs. ϕ (inset - τ s vs. $|\phi - \phi_c|$). Critical exponents calculated from HB scaling are (a) monodisperse: $\Delta = 1.3 \pm 0.23$, and $\Gamma = 1.6 \pm 0.43$; (b) bidisperse: $\Delta = 1.4 \pm 0.4$, and $\Gamma = 1.0 \pm 0.4$. Error bars include statistical and systematic errors from fits.

the shear history of the fluid micro-structure [6, 7], which would affect the scaling behavior of τ vs. $|\phi - \phi_c|$. Also, if indeed there are subtle wall-slip effects, then this artifact would preferentially affect the data at higher shear-rates [8], i.e., the data which directly influence τ and Γ. In general, we suspect that the Herschel-Bulkley scaling analysis is optimally employed for volume fractions above jamming but very close to the jamming point, which is not optimized in our macro-rheological samples.

VI. DIFFERENT SCALING OF DIMENSIONLESS MODULI VS. FREQUENCY DATA

Different damping mechanism in our colloidal suspension will result in different scaling parameter for the dimensionless frequency in the oscillatory measurements. In Fig. 7 in the main text, the frequency, ω, is scaled by $E|\phi - \phi_J|^{3/2}/\eta_s$ as other measurements suggest the drag force of the solvent is the dominating damping mechanism in our systems. However, we also explore the possibility of scaling ω by $E|\phi-\phi_J|/\eta_s$, as shown in Fig. S7, for the condition where the viscoelastic contacts between particles are the dominating damping mechanism. We found similarly good collapse as that in Fig. 7 in the main text. Unfortunately, we cannot unambiguously determine which damping mechanism plays the dominant role in our system.

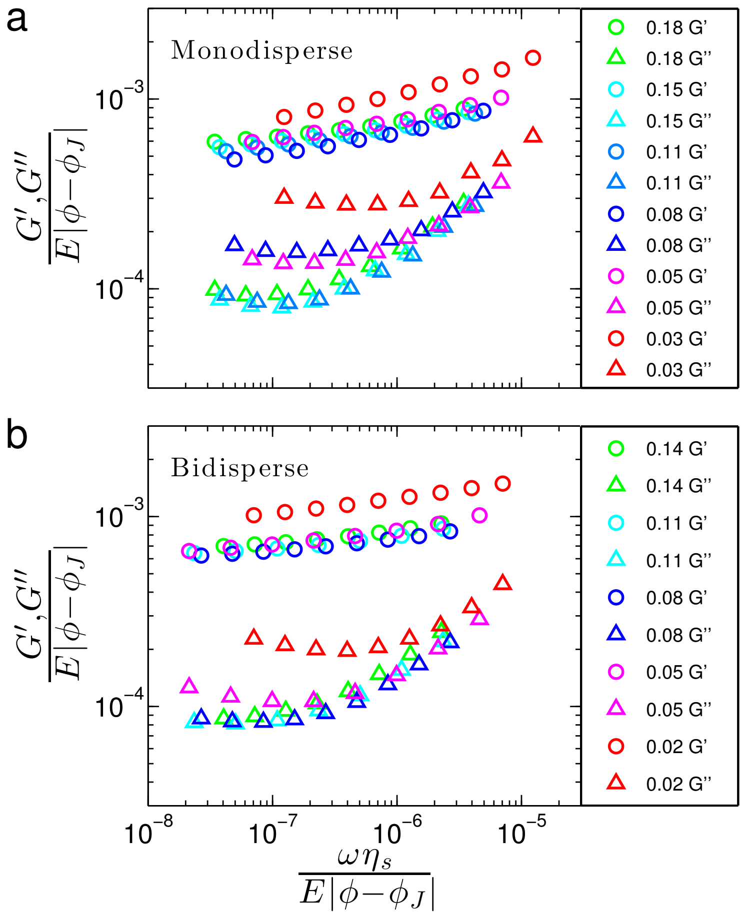

(a)

FIG. S7: (Color Online) Volume-fraction-difference-scaled dimensionless moduli, G'/E and G''/E, as function of dimensionless oscillatory frequency, $\omega\eta_s/E$ for (**a**) monodisperse and (**b**) bidisperse PNIPAM microgel spheres at $\phi-\phi_J>0$, assuming Hertzian interactions.

VII. G', G'' VS. ω DATA FOR THE BIDISPERSE PNIPAM SAMPLE AT VOLUME FRACTIONS *BELOW* ϕ_c

Fig. S8 shows elastic and viscous shear moduli for the bidisperse PNIPAM suspension (diameters, ~500 nm, ~700 nm) in liquid state, as function of oscillation frequency.

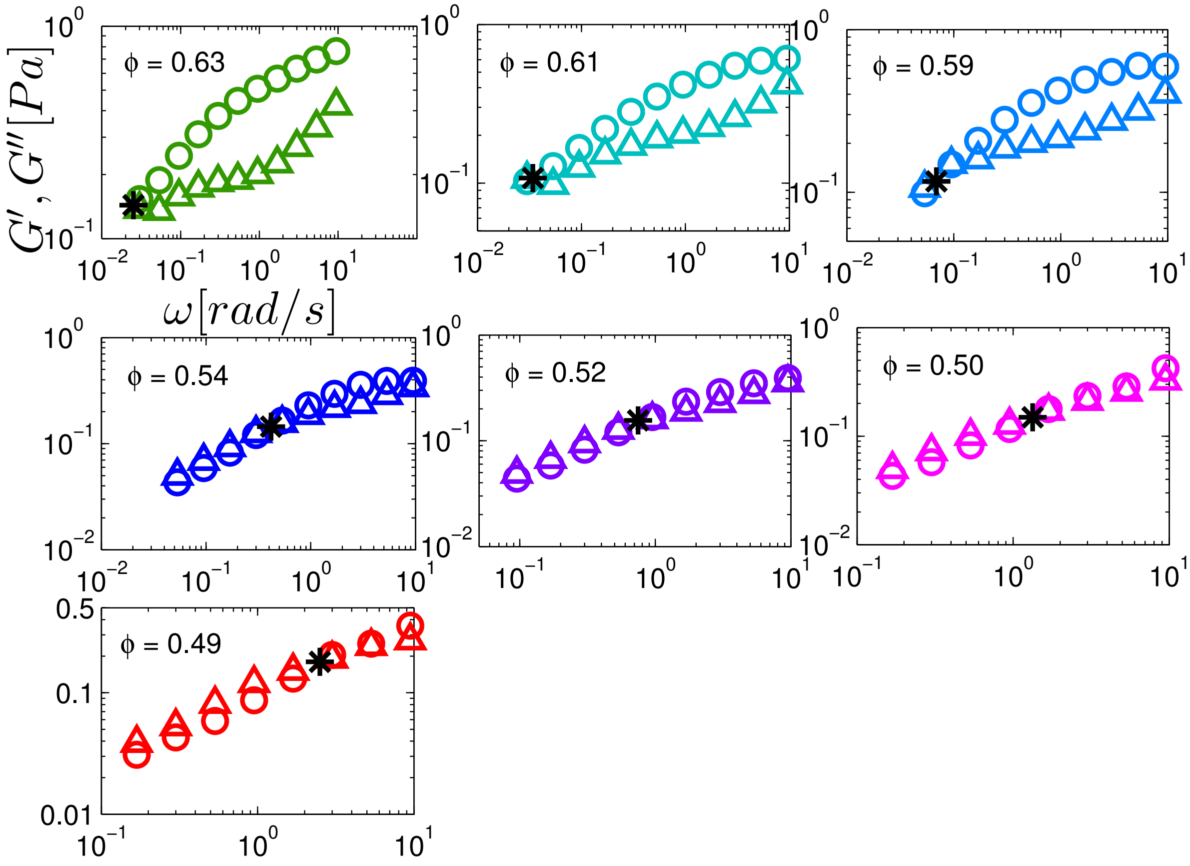

FIG. S8: (Color online) G', G'' vs. ω for the bidisperse PNIPAM suspension at different ϕ, all below ϕ_c. In all sugfigures, x-axes are ω rad/s, and y-axes are G' Pa (circles) and G'' Pa (triangles). The G'-G'' cross-over moduli are marked by black asterisks, and the corresponding frequencies give $\omega_\times$.

Cross-over frequency, $\omega_\times$ is defined as the frequency at which G' equals G''. To extract $\omega_\times$, G' and G'' vs. ω are fitted to arbitrary, high-order polynomial functions. The frequency at which the polynomial functions intersect is $\omega_\times$. The cross-over moduli corresponding to $\omega_\times$ are indicated by black asterisks at each packing fraction in Fig. S8.

VIII. DESCRIPTION OF FILES CONTAINING RAW DATA USED IN FIG. 2 AND FIG. 5 IN THE MAIN TEXT

A. Raw data for Fig. 2

visc_mono.dat: data for mono-disperse samples shown in Fig. 2a

visc_bi.dat: data for bi-disperse samples shown in Fig. 2b

Both files are in comma-seperated values (CSV) format and each row contains values of shear rate ($\dot{\gamma}$), stress (σ), and temperature (T) in the units of s^{-1}, Pa, and K, respectively.

B. Raw data for Fig. 5

osc_mono.dat: data for mono-disperse samples shown in Fig. 5a

osc_bi.dat: data for bi-disperse samples shown in Fig. 5b

Both files are in comma-seperated values (CSV) format and each row contains values of frequency (ω), storage modulus (G'), loss modulus (G'')and temperature (T) in the units of rad/s, Pa, Pa, and K, respectively.

[1] K. N. Nordstrom, E. Verneuil, W. G. Ellenbroek, T. C. Lubensky, J. P. Gollub and D. J. Durian, *Phys. Rev. E*, 2010, **82**, 041403.

[2] K. N. Nordstrom, E. Verneuil, P. E. Arratia, A. Basu, Z. Zhang, A. G. Yodh, J. P. Gollub and D. J. Durian, *Phys. Rev. Lett.*, 2010, **105**, 175701.

[3] R. C. Sonntag and W. B. Russel, *Journal of Colloid and Interface Science*, 1986, **113**, 399 – 413.

[4] G. Petekidis, D. Vlassopoulos and P. N. Pusey, *Journal of Physics: Condensed Matter*, 2004, **16**, S3955.

[5] G. Katgert, B. P. Tighe, M. E. Möbius and M. van Hecke, *Europhys. Lett.*, 2010, **90**, 54002.

[6] P. C. F. Moller, J. Mewis and D. Bonn, *Soft Matter*, 2006, **2**, 274–283.

[7] K. Martens, L. Bocquet and J.-L. Barrat, *Phys. Rev. Lett.*, 2011, **106**, 156001.

[8] R. Larson, *The Structure and Rheology of Complex Fluids*, OUP USA, 1999.